ORIGINAL ARTICLE

Enhancing seismic performance of buckling-restrained brace frames equipped with innovative bracing systems

Benyamin Mohebi[1] · Mohammad Sartipi[1] · Farzin Kazemi[2,3]

Abstract

Nowadays, to improve the performance of conventional bracing systems, in which, buckling in the pressure loads is the main disadvantage, the buckling-restrained brace (BRB) is introduced as a solution. In this study, the performance of the BRB system was improved with innovative lateral-resisting systems of double-stage yield buckling-restrained brace (DYB), and a combination of DYB improved with shape memory alloy (SMA) materials (DYB$_{SMA}$). The proposed systems have been verified and implemented in the 2- to 12-story elevation steel buckling-restrained brace frames (BRBFs). To evaluate their effects on the seismic performance, two types of analysis including nonlinear dynamic analysis (NDA) and incremental dynamic analysis (IDA) were performed considering design-based earthquakes (DBE) and maximum considered earthquakes (MCE) levels for far-field ground motions. The results showed that the BRB system in all BRBFs had the highest values of residual drift ratio (RDR$_{Med}$) demands, while implementing innovative DYB$_{SMA}$ can considerably reduce the values of RDR$_{Med}$ compared to other lateral-resisting systems. In addition, under MCE level, the BRB-DYB$_{SMA}$ system had lower values of the interstory drift ratio (IDR$_{Med}$) and RDR$_{Med}$ demands (e.g., the IDR$_{Med}$ reduced by 79.67% and 18.5% compared to BRB and DYB systems, respectively), and can be introduced as the best lateral-resisting system. Therefore, the proposed BRB-DYB$_{SMA}$ system can effectively reduce the IDR$_{Med}$ and RDR$_{Med}$ demands, as result, higher performance levels can be achieved, as well as, the collapse probability occurrence over 1 and 50 years impressively decreased.

Keywords Buckling-restrained brace frames · Double-stage yield buckling-restrained brace · Shape memory alloys · Seismic retrofit · Seismic performance assessment

1 Introduction

A buckling-restrained brace (BRB) typically consists of a ductile steel core and is designed for both tension and compression. It is imperative that the steel core be placed inside a steel casing before mortar or concrete is poured into it in order to avoid global buckling when compressed. In order to reduce the axial force between steel core and mortar, a nonbonding material or air gap will be provided. A further

advantage of the gap is that it allows for the expansion of the steel core when it is compressed. Traditional BRBs are often heavy, as a result hard to transport, lift, and installation, as they employ steel tubes filled with concrete or mortar. Decreasing the length of BRB to reduce the weight of BRB had negative effects on the failure of BRB [1]. Since the main problem of BRB is the high amount of weight, Mortezagholi and Zahrai et al. [2] proposed a less-weighted BRB model with continuous and discontinuous mortar casing. Some studies proposed a reduced-length BRB element to overcome the weight issue [1, 3].

The development of all-steel BRBs with large ductility capacities has been undertaken to avoid such a weight disadvantage [4]. In addition to the fact that all BRB components are fabricated from steel, the processing quality of the brace member is also controlled with accuracy, as well as its self-weight [5, 6]. Some experimental studies were done to investigate and confirm the behavior of all-steel BRBs [4, 7]. It was shown that the traditional BRB elements suffer from low

✉ Farzin Kazemi
farzin.kazemi@pg.edu.pl

1 Faculty of Engineering and Technology, Imam Khomeini International University, Qazvin, Iran

2 Faculty of Civil and Environmental Engineering, Gdańsk University of Technology, ul. Narutowicza 11/12, 80-233 Gdansk, Poland

3 Deptment of Civil, Environmental & Geomatic Engineering, University College London, London, UK

post-yield stiffness, which is the main issue for a large permanent drift ratio known as residual interstory drift [8–10]. The superior hysteretic characteristics of steel can allow BRBs to demonstrate stable hysteretic behavior to dissipate energy. Zhang et al. [11] proposed multiple round steel core bars that can be used to improve the strength of BRBs which are constructed using steel bars with roll-threaded screw ends. This will overcome the limitations of single-bar core BRBs [12]. To improve the accuracy of experimental evaluations of reinforced concrete frames equipped with BRBs, a loading protocol was proposed by Bai et al. [13] to estimate the seismic performance of these frames taking variable axial loads into account. Considering that the core material of BRBs greatly influences the hysteretic behavior of BRBs, Zhang et al. [14] have investigated auxetic metamaterials as core materials for BRBs with different shapes to assess the hysteretic behavior of auxetic metamaterials under cyclic load conditions.

Double-stage yield buckling-restrained brace (DYB) employs a multi-sectional BRB cores in a double-stage yield strategy. While small core plate of BRB yields earlier than large one, the braced frame can minimize its response to low- to mid-level ground motions due to the dissipation of energy caused by early yielding. There are no additional welding requirements for the DYB, as the composition is similar to that of the conventional BRB. As well, the steel casing of DYB could be reused several times as well as the core plate could be repaired or replaced by disassembling the bolts [15]. An investigation was made into three key parameters of the strengthening ratio for strengthened sections, the length ratio for yield sections, and the bearing capacity ratio for yield sections [16]. It should be noted that the failure concentration in the core of BRB can be avoided using some innovative stoppers. There is a consequence of residual deformation in the building that involves costly repair work and long-term interruption of building operations. The geometrical properties of shape memory alloy (SMA) bars were optimized in order to improve the self-centering ability of BRBs [17, 18].

Recently, SMA materials have been used in bracing system to improve the capability of them in reducing the residual displacements. Using a probabilistic approach, Shi et al. [19] investigated the seismic performance of steel buildings equipped with SMA-based self-centering bracing systems. Their results confirm that the proposed brace reduced likelihood of reaching damage states linked to residual drifts particularly for high-return-period seismic events. Moreover, some comprehensive investigations have been done to perform seismic risk and performance assessment [20] and failure behavior of SMA-based braces [21]. Moreover, they provided insights into the seismic and collapse performance of reinforced concrete (RC) structures braced with BRBs, considering the ultimate deformation capacity of

the BRBs on seismic response and collapse mode. Their results showed that BRB can assure an ultimate deformation safety coefficient of 1.2 [22]. Shi et al. [23] performed experimental tests to examine hybrid self-centering brace responses under increased loading displacement. Loading rate and training cycle's effects on mechanical behavior are studied, and low-cycle fatigue evaluated on two braces up to 30 cycles at large displacement. The hybrid self-centering braces with SMA technology offer an average of 9% equivalent viscous damping across various loading amplitudes, showcasing a robust self-centering attribute.

A DYB, which has a hysteresis loop designed to promote the spread of damages, was used by Barbagallo et al. [24] to improve the seismic performance of conventional steel braces. Apart from the examples given above, it has also been found very promising to utilize various damping mechanisms, including buckling-restrained brace frames (BRBFs) paired with moment-resisting frames [25], BRBs paired with high-damaging rubber dampers [26], steel bending plates with SMA bars [27], and ring spring dampers paired with viscous dampers [28].

Nowadays, in the seismic-prone area, an increasing number of BRBs were implemented in the structures as a lateral force-resisting system. Conventional BRBs are mostly designed based on the elastic behavior in the low-cycle excitations; thus, they cannot help to dissipate seismic energy in the most frequently happened earthquakes, e.g., especially those with lower magnitudes, while they can add more lateral stiffness to the system and reduce the fundamental period of structures. Therefore, there is a need to have strategy for dissipating the energy of the earthquakes with lower magnitudes. To overcome this issue, in this study, economical and reliable alternatives are proposed to increase the performance of BRB systems implemented in buildings. In addition, the DYB system and DYB improved with SMA materials (DYB_{SMA}) are proposed to implement in structures to provide a complete lateral force-resisting system for dissipating energy in any stage of seismic excitations. Therefore, it is possible to dissipate energy in any type of seismic events and prevent structural damages. Moreover, this study evaluates the possible retrofitting strategy of BRB systems, in which, the novel lateral force-resisting systems are investigated.

2 Modeling process

2.1 Mechanism of DYB and DYB$_{SMA}$

In this section, the mechanism of the proposed DYB and DYB$_{SMA}$ are explained. The DYB has two stages of small and large parts, in which, the small part can be active in seismic excitation with lower frequencies to dissipate energy, and after

experiencing a large amount of displacement, the large part is activated. To control the deformation of a small part, there should be a gap element between two parts, and to define this gap, the suggested solution by Barbagallo et al. [24] presented in Fig. 1 can be employed.

Figure 1 presents the geometry of DYB element used in this research. To define the actual behavior of DYB, the parameters of the length of small and large segments, L_{CS} and L_{CL}, length of the middle segment, L_{CM}, length of connection segments for small and large parts, L_{JS} and L_{JL}, and length of transition segments for small and large parts, L_{TS} and L_{TL}, were defined. For each segment, corresponding cross-sectional areas were determined assuming the thickness of the core, t. To have a good performance of DYB, the L_{CS} and L_{CL} were determined to be equal to 12% and 43% of the total length of the brace, and L_{JS} and L_{JL} were determined to equal 15% of the total length of the brace. To validate the modeling of DYB, the experimental work performed by Sun et al. [15] (see DYB-3 details in the reference [15]) was used. According to details presented in the experimental work, the material yield strength, F_y, ultimate strength, F_u, and Young's modulus, E_s, were selected as 260 MPa, 362 MPa, and 2.07×10^5 MPa, respectively. The total length of the DYB is equal to 4 m, and small and large parts are equal to 0.45 m and 1.68 m, respectively, assuming the middle stopper of 0.338 m and the core thickness of 30 mm.

Two nonlinearBeamColumn elements are arranged in parallel, linking two ends of DYB to the intermediate node showed in Fig. 1. While the cross-sectional area of two BRB parts is variable, an equivalent cross-sectional area is attributed to each element. The equivalent area of the smaller BRB, denoted as $A_{eq,S}$, and the larger BRB, denoted as $A_{eq,L}$, are computed using the following formula:

$$A_{eq,S} = \frac{A_{CS}}{\frac{L_{JS}.A_{CS}}{L_{WS}.A_J} + \frac{L_{TS}.A_{CS}}{L_{WS}.A_{TS}} + \frac{L_{CS}}{L_{WS}}} \tag{1}$$
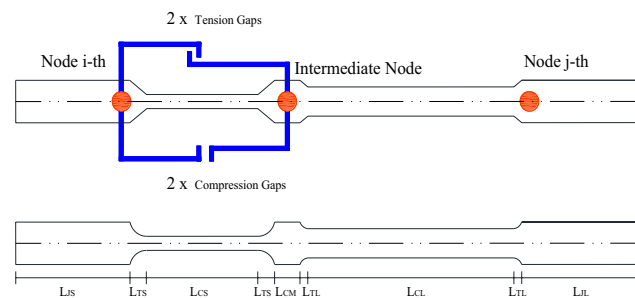
$$A_{eq,L} = \frac{A_{CL}}{\frac{L_{JL}.A_{CL}}{L_{WL}.A_J} + \frac{L_{TL}.A_{CL}}{L_{WL}.A_{TL}} + \frac{L_{CL}}{L_{WL}}} \tag{2}$$

where the A_{CS}, A_J, A_{TS}, A_{CL}, and A_{TL} denote the cross-section area of the different sections of DYB presented in Fig. 1.

Two yielding segments, along with their corresponding transition and connection segments referred to as the small BRB and large BRB, exhibit behavior analogous to two conventional BRBs connected in a series arrangement. The buckling-restraint mechanism is attached to the external connection segment of the small BRB through the use of bolts and elongated holes. For activating the small part of DYB and controlling the total allowable deformation of the core, the short and long slotted holes of 5 mm and 40 mm are considered, respectively. To define the loading protocol, the maximum allowable axial deformation (i.e., 40 mm) divided by the total length (i.e., 4 m) was selected as the final stage of loading protocol (i.e., 1%), and five stages were defined to reach this stage, in which, in each stage, the maximum deformation doubled. Figure 2 presents the loading protocol used for validating the DYB and axial force–deformation curve of DYB model used in this research. Specifically, the displacement ratio, denoting the proportion of the imposed axial displacement to the length of the DYB, was elevated from 1/2000 to 1/100.

According to Fig. 1, two tension gaps were defined using elastic perfectly-plastic gap (i.e., *ElasticPPGap*), in which, the first one known as the flexible tension gap and will be active in the clearance distance of small holes, and the second one known as the stiff tension gap will have infinitive stiffness and larger gap size compared to the flexible tension gap. For modeling the behavior of the cores of DYB, *Steel02* material has been used with parameters of $CR_1 = 0.925$, $CR_2 = 0.15$, $a_1 = 0.02$, $a_2 = 1.0$, $a_3 = 0.009$, and $a_4 = 1.0$ [29]. The pinching behavior typically involves strength and stiffness degradation during cyclic loading. This model should represent the cyclic behavior of the DYB's force–displacement response during loading and unloading cycles. The parallel use of tension gaps and corotational truss element (i.e., *corotTruss*) has confirmed the simulation of the pinching behavior observed in the experimental test. On the other side, the compression gaps can be activated in the compression load for shortening the small part of DYB. The cross-sectional area of the considered gaps is the same, while the stiff tension gap has 1.7 times the size of the flexible tension gap and a large value of stiffness (i.e., 1000 times) of the flexible tension gap [24]. Comparison of result of experimental and numerical analysis illustrates that the modeling process has acceptable accuracy for modeling DYB element. In addition, the proposed element can accurately model the ultimate cyclic behavior of small and large segments of

Fig. 1 Numerical modeling of DYB with defining gaps for a small part
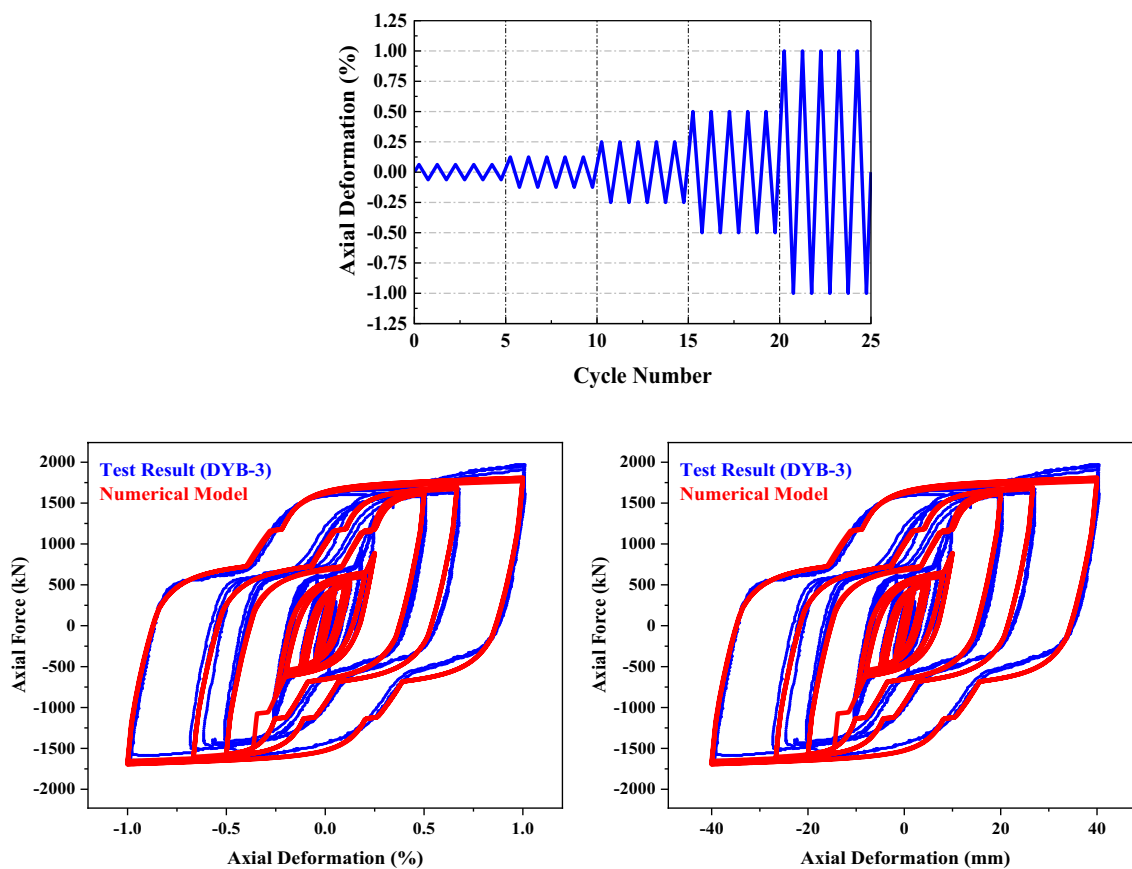
Fig. 2 Loading protocol used for validating the DYB, and axial force–deformation curve of DYB model used in this research and the test result considering the percentage and actual deformations [15]

DYB. Moreover, the pinching behavior of the experimental test was correctly determined by numerical modeling.

To improve the capability of DYB, the SMA material was used in the large segment to be activated after reaching the pinching behavior of the small segment. Since the main issue of using DYB in structures is the large residual drift, the idea of using SMA material in the large part stems from the self-centering capability of this material to control the residual drift. To model the SMA brace, 25% of base shear was considered to calculate the length and area of SMA used in DYB. To calculate the parameters, the material used by Qiu and Zhu [30] was used. According to the procedure of modeling SMA brace for frames, for an inverted V-bracing system, the area and length of SMA core, A_{SMA} and L_{SMA}, can be calculated as follows:

$$A_{SMA} = \frac{\sum_{j=i}^{n} C_j V_{base}}{2\cos\theta_i . \sigma_{SMA}} \tag{3}$$

$$L_{SMA} = \frac{E_{SMA}.\theta_y(h_i - h_{i-1})\cos\theta_i}{\sigma_{SMA}}, \quad h_0 = 0 \tag{4}$$

where the E_{SMA} and σ_{SMA} are equal to 50 MPa and 500 MPa, respectively, according to the lowest temperature of SMA material. C_j, h_i and θ_i show the lateral load pattern, the story height and the brace angle corresponding to the floor level i. To determine the yield interstory drift, θ_y, the peak interstory drift should be divided into the ductility demand that is assumed equal to 5.0. To control the accuracy of SMA materials modeled in structures, the procedure for validating the self-centering behavior of SMAs conducted by Kazemi and Jankowski [31] was used. According to this research, the SMA-based BRB element was verified and implemented on the BRBFs.

2.2 Modeling of buildings

To investigate the capability of DYB and DYB_{SMA} for enhancing the performance of BRBFs, the symmetric plan presented in Fig. 3 was selected for modeling 2 to 12-story elevation buildings. It was assumed that the outer frames
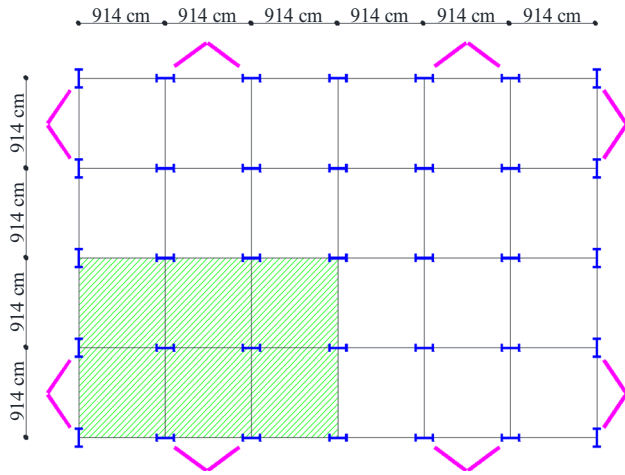
Fig. 3 Symmetric plan for modeling of buildings

that consist of two bays of BRBFs have lateral-resisting systems, while other columns of buildings are assumed as gravity columns. Therefore, in each direction, each bay of BRBFs has to control lateral loads of green area shown in Fig. 3, and the total lateral loads of each direction were divided between two outer BRBFs. The height of structures assumed as 3.96 m for all floor levels. To design the BRBFs, the ASCE 7-10 [32], AISC 360-10 [33], and AISC 341-10 [34] provisions were used assuming the buildings located in California having soil type D, given S_{DS} and S_{D1} of 1.25 g and 0.6 g, respectively. To model buildings, the yield and ultimate stress of 344.74 MPa and 448.16 MPa were selected for steel materials of columns and beams, respectively. In addition, for core plates of braces, the yield stress of 289.58 MPa was assumed. All buildings were modeled in ETABS 2016 software considering the parameters of $R = 8$,

Table 1 Abbreviations and acronyms list used in the research

Abbreviation	Description
BRB	Buckling-restrained brace
DYB	Double-stage yield buckling-restrained brace
SMA	Shape memory alloy
BRBFs	Buckling-restrained brace frames
DYB_{SMA}	DYB improved with shape memory alloys
NDA	Nonlinear dynamic analysis
IDA	Incremental dynamic analysis
DBE	Design-based earthquake level
MCE	Maximum considered earthquake level
IDR	Interstory drift ratio
RDR	Residual drift ratio
IDR_{Med}	Median of interstory drift ratio
RDR_{Med}	Median of residual drift ratio
DCF	Drift concentration factor
CMR	Collapse margin ratio
L_{CS}	Length of small segment
L_{CL}	Length of large segment
L_{CM}	Length of middle segment
L_{JS}	Length of connection segments for small part
L_{JL}	Length of connection segments for large part
L_{TS}	Length of transition segments for small part
L_{TL}	Length of transition segments for large part
t	Thickness of the core
F_y	Material yield strength
F_u	Material ultimate strength
E_s	Young's modulus
A_{SMA}	Area SMA core
L_{SMA}	Length of SMA core
$\delta_{max,floor\,i}$	Maximum interstory drift of the floor level
$\delta_{max,roof}$	Maximum drift of roof
$Sa(T_1)$	Spectral acceleration at fundamental period of structures
Sa_{MCR}	Spectral acceleration at design spectrum under the MCE level
λ_{Col}	Mean annual frequency of collapse

$C_d = 5$, and $\Omega_0 = 2.5$. Table 1 illustrates the designed members of BRBFs assuming selected lateral-resisting systems. To model DYB_{SMA}, the area of SMAs presented in Table 2 increased four times.

In an attempt to model three-dimensional buildings in OpenSees [29] software, researchers employed some approaches to model two-dimensional frames (for example see [35, 36]). The principal analytical tool for analyzing the deterioration of structural elements is able to model

Table 2 Beam, columns, and BRB members for 2- to 12-story structures with selected lateral-resisting systems

Model	Floor	Column	Beam	BRB (cm^2)	DYB			BRB-DYB$_{SMA}$	
					A_{equal} (cm^2)	Small (cm^2)	Large (cm^2)	BRB (cm^2)	SMA (cm^2)
2-Story	1st	W10X45	W14X38	19.35	25.8	10.96	21.93	19.35	5.16
	2nd	W10X45	W14X38	12.9	16.13	7.1	13.54	12.9	3.87
4-Story	1st	W14X82	W16X45	25.8	32.25	13.54	27.1	25.8	7.74
	2nd	W14X82	W16X45	22.58	29.03	12.25	24.51	22.58	6.45
	3rd	W12X45	W14X38	19.35	25.8	10.96	21.93	19.35	5.16
	4th	W12X45	W14X38	9.67	12.9	5.16	10.32	9.67	3.87
6-Story	1st	W14X132	W16X45	29.03	35.48	14.83	29.67	29.03	8.38
	2nd	W14X132	W16X45	29.03	35.48	14.83	29.67	29.03	7.74
	3rd	W14X82	W16X45	25.8	32.25	13.54	27.1	25.8	6.45
	4th	W14X82	W14X38	22.58	29.03	12.26	24.51	22.58	5.16
	5th	W12X45	W14X38	16.13	22.58	9.03	18.7	16.13	3.87
	6th	W12X45	W14X38	9.67	12.9	5.16	10.32	9.67	2.58
8-Story	1st	W14X159	W16X50	32.25	41.93	17.41	34.83	32.25	9.67
	2nd	W14X159	W16X50	32.25	38.7	16.13	32.25	32.25	9.03
	3rd	W14X132	W16X50	32.25	38.7	16.13	32.25	32.25	7.74
	4th	W14X132	W16X45	29.03	35.48	14.83	29.67	29.03	7.1
	5th	W14X82	W16X45	25.8	32.25	13.54	27.1	25.8	6.45
	6th	W14X82	W16X40	19.35	25.8	10.96	21.93	19.35	5.16
	7th	W12X45	W16X40	16.13	22.58	9.03	18.7	16.13	3.87
	8th	W12X45	W16X40	9.67	12.9	5.16	10.32	9.67	2.58
10-Story	1st	W14X176	W18X60	9.67	48.38	20	40.64	9.67	10.32
	2nd	W14X176	W18X60	16.13	45.16	18.7	37.41	16.13	9.67
	3rd	W14X159	W18X60	22.58	45.16	18.7	37.41	22.58	9.03
	4th	W14X159	W18X60	29.03	45.16	18.7	37.41	29.03	8.38
	5th	W14X132	W18X55	32.26	41.93	17.41	34.83	32.26	7.74
	6th	W14X132	W18X55	35.48	38.7	16.13	32.25	35.48	7.1
	7th	W14X82	W18X46	38.7	35.48	14.83	29.67	38.7	6.45
	8th	W14X82	W18X46	38.7	29.03	12.25	24.51	38.7	5.16
	9st	W12X45	W18X46	38.7	22.58	9.03	18.7	38.7	3.87
	10st	W12X45	W18X46	41.93	12.9	5.16	10.32	41.93	2.58
12-Story	1st	W12X211	W21X68	48.38	58.06	24.51	48.38	48.38	10.96
	2nd	W12X211	W21X68	48.38	58.06	24.51	48.38	48.38	10.32
	3rd	W14X193	W21X68	48.38	54.83	22.58	45.8	48.38	9.67
	4th	W14X193	W21X68	48.38	54.83	22.58	45.8	48.38	9.67
	5th	W14X159	W21X68	45.16	51.61	21.29	43.22	45.16	9.03
	6th	W14X159	W21X68	45.16	51.61	21.29	43.22	45.16	8.38
	7th	W14X132	W18X60	41.93	48.38	20	40.64	41.93	7.74
	8th	W14X132	W18X60	35.48	41.93	17.41	34.83	35.48	7.1
	9st	W12X96	W18X60	32.25	38.7	16.13	32.25	32.25	6.45
	10st	W12X96	W18X46	29.03	32.25	14.83	29.67	29.03	5.16
	11nd	W12X45	W18X46	25.8	25.8	10.96	21.93	25.8	3.87
	12rd	W12X45	W18X46	16.12	16.13	7.1	13.54	16.12	2.58

the deterioration of strength and stiffness. Two-dimensional modeling can be accomplished using this tool. In this research, the BRBF located in the Y direction was selected for two-dimensional modeling in OpenSees [29] software. According to approaches, all columns will be modeled as part of the leaning column [37], ignoring the columns that will be modeled as part of the BRBFs (e.g., see [38]). In this study, it was shown that OpenSees [29] software is capable of modeling structural elements with high accuracy, in addition to providing a significant increase in analysis time and a reduction in computational effort. The result of fundamental periods achieved from ETABS 2016 software, which was considered to model three-dimensional buildings, was used to validate the two-dimensional models. The rigid truss element was used to connect the nodes at the beginning and end of the beam for each floor, thereby creating a rigid diaphragm. Furthermore, on each floor, a rigid truss element was used to connect the braced bay to the leaning column [39]. During the modeling process, a nonlinear beam-column element served as the brace core, while two elastic beam-column elements were used as elastic segments at the start and end of the brace. This method of modeling has been verified by a previous study [8–10]. In addition, the procedure of modeling the BRB, DYB, and DYB_{SMA} were employed to model these elements in OpenSees [29] software.

In this research, all BRBFs have been designed based on the ASCE 7-10 [32], AISC 360-10 [33], and AISC 341-10 [34], which are considered as benchmark. Assuming the retrofitting strategy with same design target, four types of BRBFs assuming BRB in both bracing bays, DYB in both bracing bays, DYB_{SMA} in both bracing bays, and BRB and DYB_{SMA} in each of the bracing bays, were modeled. It should be noted that o investigate the capability of DYB and DYB_{SMA} for enhancing the performance of BRBFs, the designing process of DYB and DYB_{SMA} introduced by Barbagallo et al. [24] and Qiu and Zhu [30] have been implemented, respectively. The schematic view of the modeling of the BRBFs is presented in Figs. 4, 5, and 6. To consider the SMAs for the large segment, the materials of small and large segments are divided in the middle connection of the DYB presented in Fig. 1. It is noteworthy that the BRBFs were considered as main lateral-resisting system and other systems were designed based on the idea of retrofitting this force-resisting system in order to achieve higher performance level. In addition, due to retrofitting strategy, to better compare the real condition of the buildings, the beams and columns kept same for all the systems since there is no possibility to change them during the retrofitting process.

3 Results of analysis

3.1 Seismic analysis

In this research, two types of analysis including nonlinear dynamic analysis (NDA) and incremental dynamic analysis (IDA) were used to compare the effectiveness of proposed
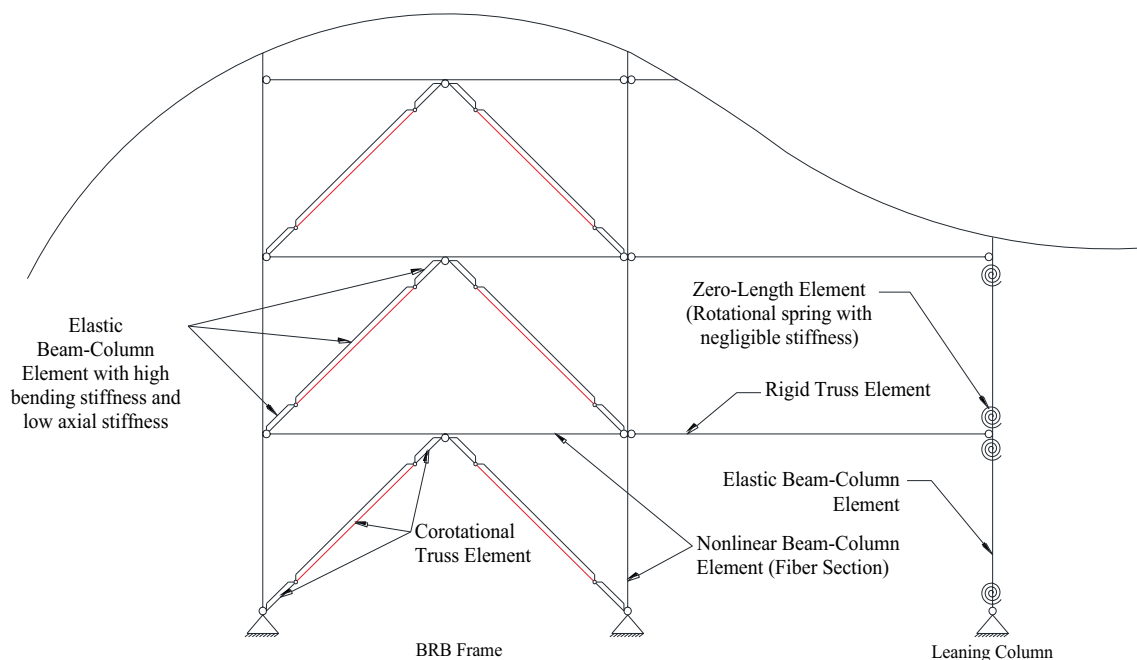
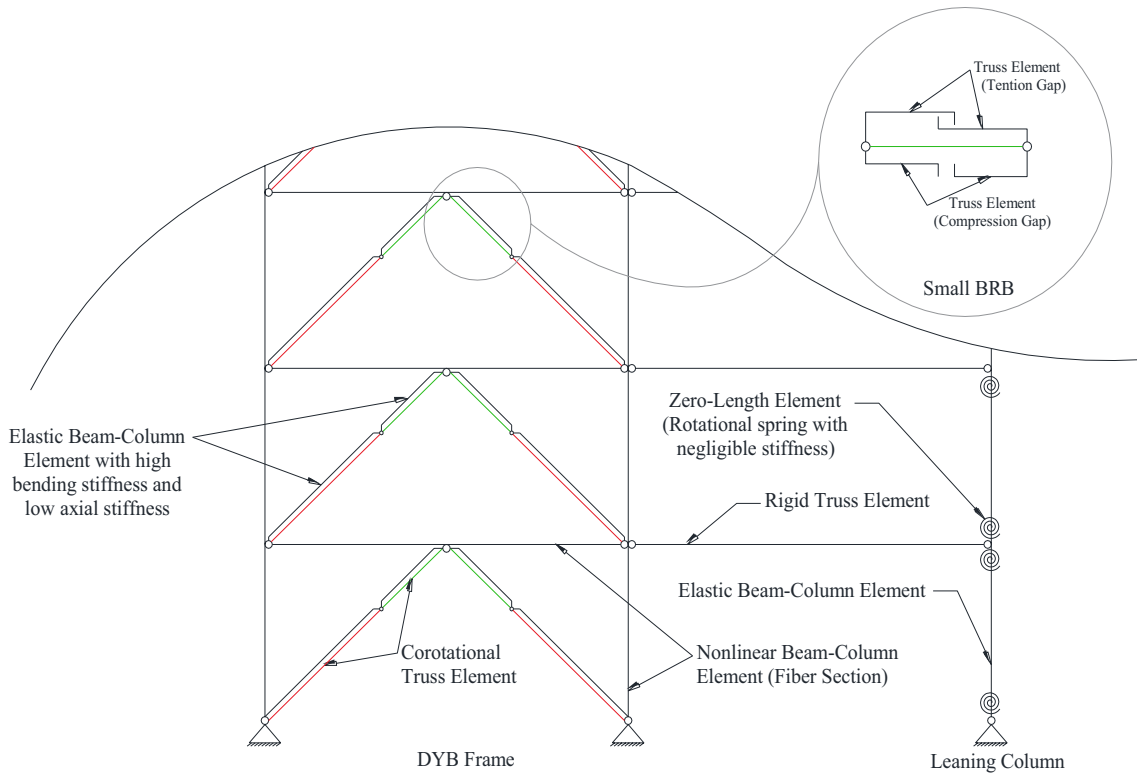**Fig. 4** Schematic view of modeling of BRB lateral-resisting system

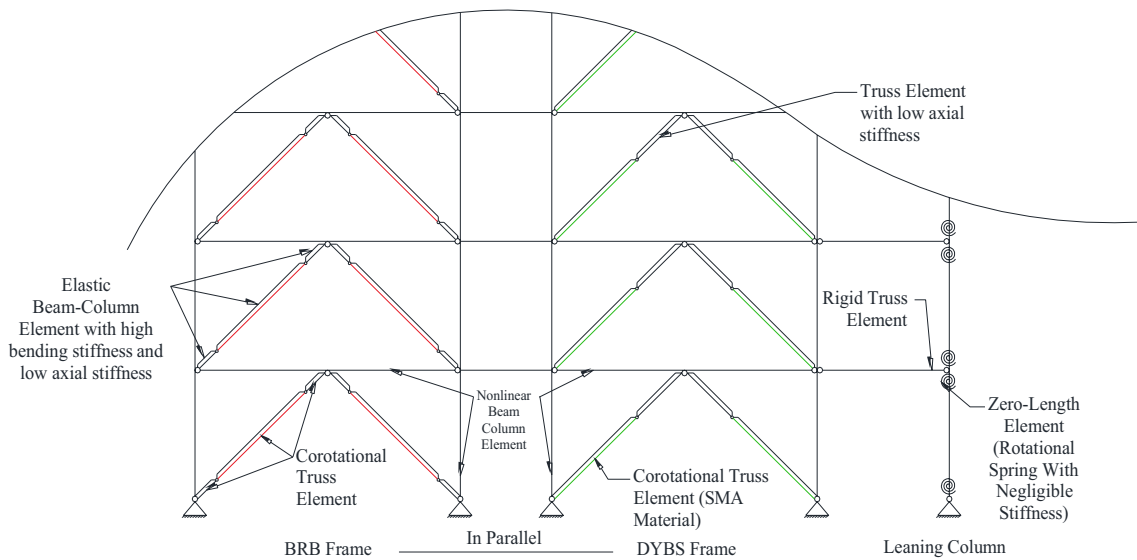**Fig. 5** Schematic view of modeling of DYB lateral-resisting system

Fig. 6 Schematic view of modeling of BRB-DYB$_{SMA}$ lateral-resisting system

systems. The NDA is an advanced computational technique employed in structural engineering to simulate and evaluate the behavior of structures subjected to seismic loads. To perform NDAs, two intensity measures of design-based earthquakes (DBE) and maximum considered earthquakes (MCE) levels have been considered. Figure 7 illustrates the DBE and MCE levels that were scaled to fit the target spectrum introduced by ASCE 7-10 [32]. The IDA is a sophisticated computational technique within the realm of structural engineering that facilitates the assessment and
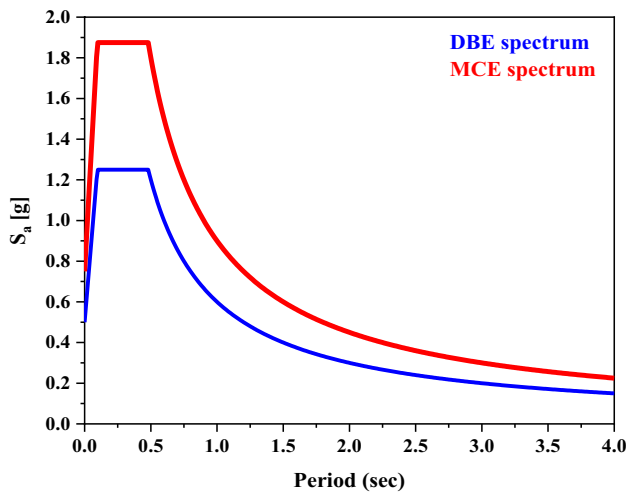
Fig. 7 DBE and MCE levels fitted to the target spectrum introduced by ASCE 7-10 [32]

comprehension of a structure's seismic performance under progressively increasing levels of ground motion intensity. Therefore, IDAs provide a more comprehensive understanding of a structure's behavior by subjecting it to a range of ground motion records [40]. To increase the effectiveness of the IDAs, the Hunt and Fill algorithm is used, which in the "hunt" phase, the algorithm starts with a small value of intensity measure and continues the analysis until collapse of structure, then in the "fill" phase, the step of analysis decreases to fill the gap between the last step and collapse state to find the exact value of intensity measure correspond the collapse capacity [41]. All these procedures have been introduced in OpenSees [29] to continue the analysis and plot the IDA curves based on the different engineering demands known as the interstory drift ratio (IDR) and residual drift ratio (RDR). Since the considered site of buildings is classified as far-field, to perform both analyses, the far-field ground motion record set which includes 44 records, has been extracted from FEMA P695 [42]. Table 3 presents the details of far-field ground motion records.

3.2 Effects of gap distance

As it was shown in Fig. 1, four gap elements (i.e., two tension and two compression gaps) connected the i-th node to the intermediate node. The tension gaps will be active in elongation and the compression gaps will control the imposed threshold given the clearance of the holes. Figure 8 illustrates axial force–deformation curve of DYB_{SMA} having different flexible tension gaps of 5.0 mm and 10.0 mm. It can be seen that the flexible gap has effective influence on controlling the deformation and transition part. Different flexible gaps will be selected to find out their effects on the seismic behavior of BRBFs. To present

Table 3 Details of far-field ground motion records [42]

Name	PEER-NGA record information			Recorded motions	
	RSN No	Magnitude	Fault	PGA max (g)	PGV max (cm/s)
Northridge	953	Northridge	Thrust	0.52	63
Northridge	960	Northridge	Thrust	0.48	45
Duzce	1602	Duzce	Strike–slip	0.82	62
Hector	1787	Hector	Strike–slip	0.34	42
Imperial	169	Imperial	Strike–slip	0.35	33
Imperial	174	Imperial	Strike–slip	0.38	42
Kobe	1111	Kobe	Strike–slip	0.51	37
Kobe	1116	Kobe	Strike–slip	0.24	38
Kocaeli	1158	Kocaeli	Strike-slip	0.36	59
Kocaeli	1148	Kocaeli	Strike–slip	0.22	40
Landers	900	Landers	Strike–slip	0.24	52
Landers	848	Landers	Strike–slip	0.42	42
Loma	752	Loma	Strike–slip	0.53	35
Loma	767	Loma	Strike–slip	0.56	45
Manjil	1633	Manjil	Strike–slip	0.51	54
Superstition	721	Superstition	Strike–slip	0.36	46
Superstition	725	Superstition	Strike–slip	0.45	36
Cape	829	Cape	Thrust	0.55	44
Chi-Chi	1244	Chi-Chi	Thrust	0.44	115
Chi-Chi	1485	Chi-Chi	Thrust	0.51	39
San	68	San	Thrust	0.21	19
Friuli	125	Friuli	Thrust	0.35	31

the effects of gap distance for modeling the small part of DYB and DYB_{SMA}, the Median of interstory drift ratio (IDR_{Med}) and residual drift ratio (RDR_{Med}) were plotted performing NDAs based on the ground motion records under MCE level. Figures 9 and 10 depict the IDR_{Med} and RDR_{Med} of the 6-story BRBF considering different values of gaps for a small part of BRB-DYB_{SMA} and DYB under the MCE level. According to Figs. 9a and 10a, it can be observed that the largest values of IDR_{Med} were determined in the first-floor level of the 6-story BRBFs assuming the gap distance equal to 15 mm, and by decreasing the gap distance, the IDR_{Med} was reduced. Comparing the results of Figs. 9b and 10b, it can be seen that increasing the gap distance in numerical models can considerably increase the RDR_{Med} in the 6-story BRBFs. By increasing the gap distance which controls the deformation of a small part of DYB, both demands of IDR_{Med} and RDR_{Med} show increasing trends. Therefore, it can be concluded that the small part of DYB plays a crucial role in controlling the IDR_{Med} and RDR_{Med} demands and the limitation gap
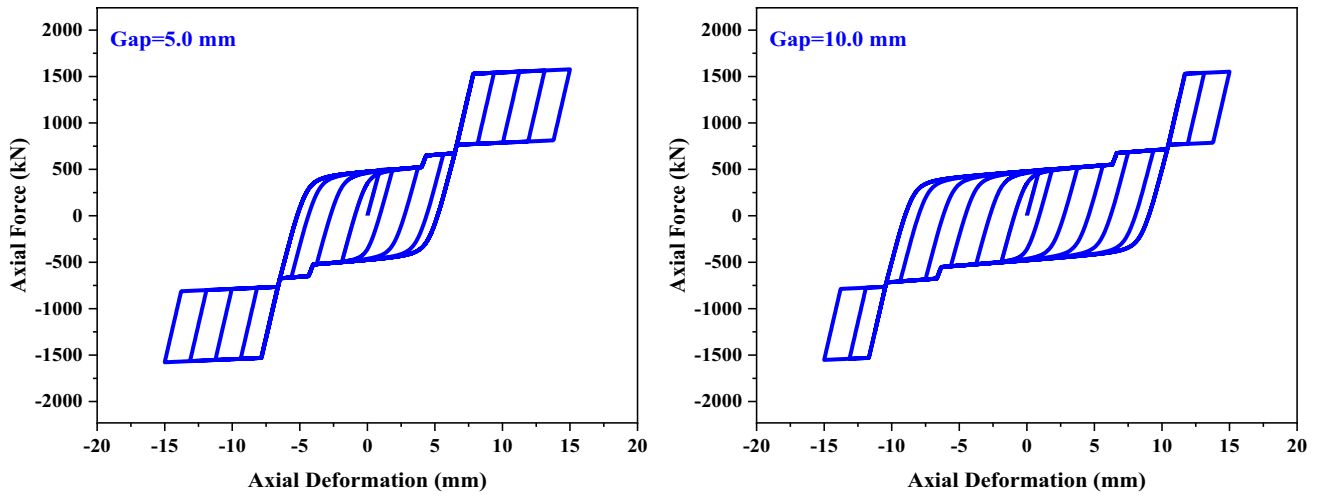
Fig. 8 Axial force–deformation curve of DYB$_{SMA}$ having different flexible tension gaps of 5.0 mm and 10.0 mm
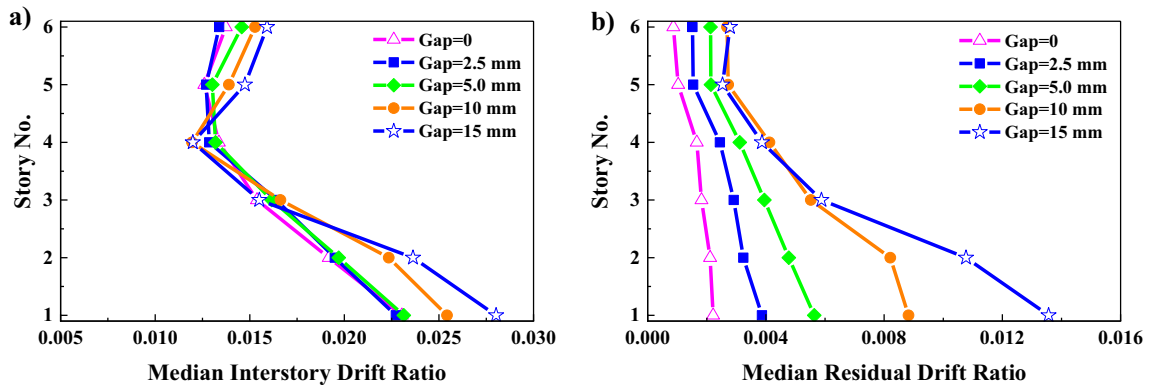

Fig. 9 IDR$_{Med}$ and RDR$_{Med}$ of the 6-story BRBF considering different values of gaps for a small part of BRB-DYB$_{SMA}$ under the MCE level
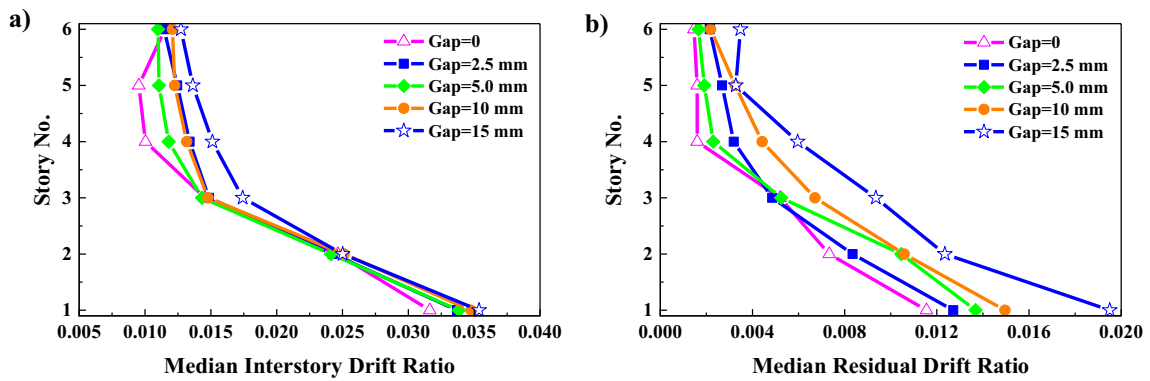

Fig. 10 IDR$_{Med}$ and RDR$_{Med}$ of the 6-story BRBF considering different values of gaps for a small part of DYB under the MCE level

distance should be assumed an appropriate value to have effective behavior.

The size of the flexible tension gap was selected equal to 5 mm and the stiff tension gap was selected 1.7 times of flexible tension gap according to Barbagallo et al. [24]. Therefore, for DYB and DYB_{SMA}, the 5 mm gap distance is considered for the small part.

3.3 Comparison of seismic performance

After selecting an appropriate gap distance for models, the modeling parameters were regulated for all BRBFs, and the NDAs were done based on the DBE and MCE levels assuming the IDR_{Med} and RDR_{Med} as demands. Figures 11 and 12 show the distribution of the IDR_{Med} and RDR_{Med} demands for all BRBFs assuming different lateral systems under the DBE level. According to the results of Fig. 11, the DYB_{SMA} has the largest values of IDR_{Med} compared to other lateral systems, which means this system experienced a great number of lateral deformations during DBE-level ground motions. Comparing the results of other lateral systems, the DYB system had lower values of IDR_{Med} in floor levels compared to BRB and BRB-DYB_{SMA} in all BRBFs. Figure 12 presents that DYB_{SMA} system had the lowest values of RDR_{Med} distributed in floor levels, which is the result of the self-centering ability of SMA materials. In addition, the BRB system in all BRBFs had the highest values of RDR_{Med} demands, which mostly occurred at the first-floor level. Moreover, the DYB system had approximately lower values compared to BRB-DYB_{SMA}.

To conclude the results, although the DYB_{SMA} had the lowest permanent deformations, this system experienced the highest values of lateral deformations under DBE-level ground motions and do not have a good performance in this demand. On the other hand, the DYB system had lower values of IDR_{Med} and RDR_{Med} demands at floor levels and showed an acceptable performance under the DBE level compared to BRB and BRB-DYB_{SMA}. Figures 13 and 14 show the distribution of the IDR_{Med} and RDR_{Med} demands for all BRBFs assuming different lateral systems under the MCE level. Similar to DBE level results, the DYB_{SMA} system had the highest values of IDR_{Med} and the lowest values of RDR_{Med}.

Although this system can significantly control the RDR_{Med} demand, the results of IDR_{Med} demands confirm that the system may experience a collapsed state since the lateral drift in some story levels crossed the allowable limitations. Therefore, this system is not recommended as a reliable lateral system. Comparing the results show that the BRB-DYB_{SMA} structures had lower values of the IDR_{Med} and RDR_{Med} demands, which shows the considerable performance of this system under MCE-level ground motions. For instance, the BRB-DYB_{SMA} in a 12-story structure can reduce the IDR_{Med} by 79.67% and 18.5% compared to
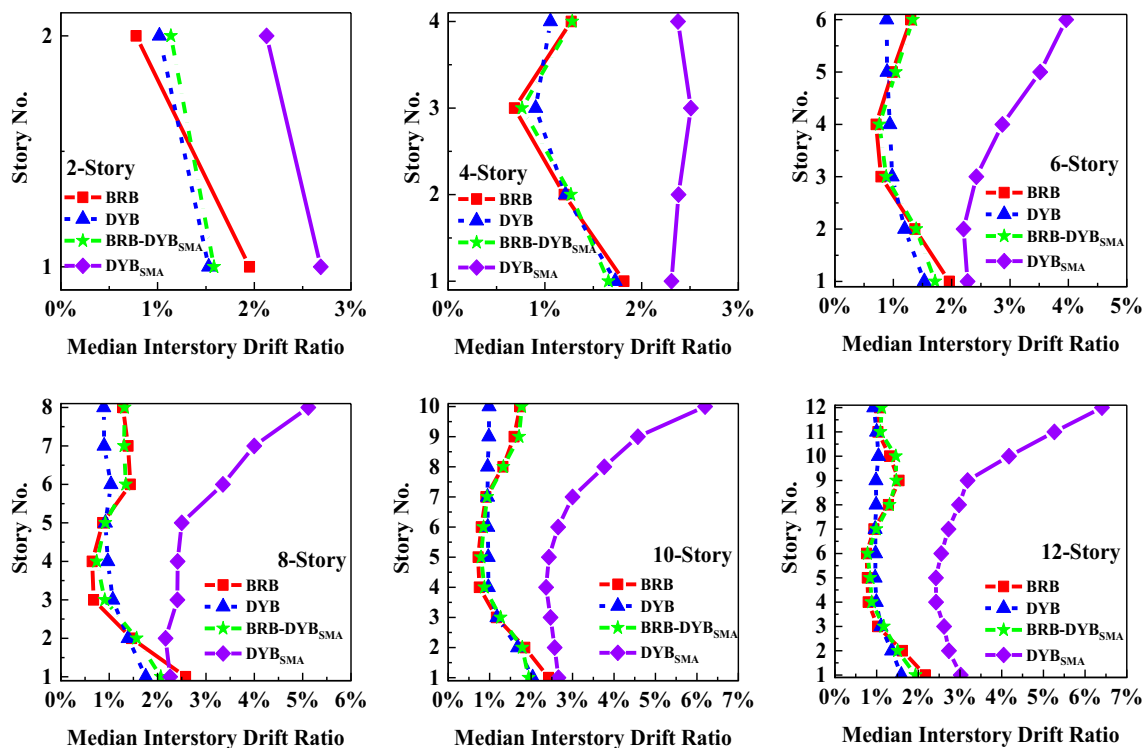

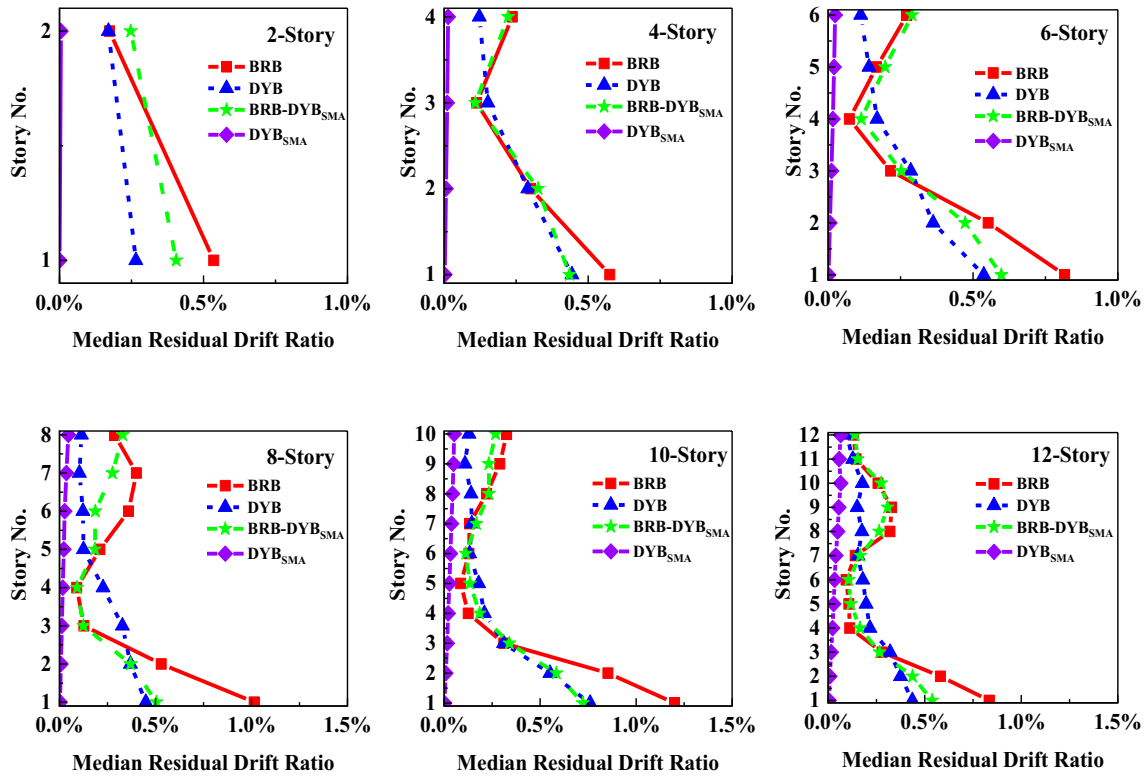**Fig. 11** IDR_{Med} of BRBFs considering different lateral systems under the DBE level

Fig. 12 RDR$_{Med}$ of BRBFs considering different lateral systems under DBE level
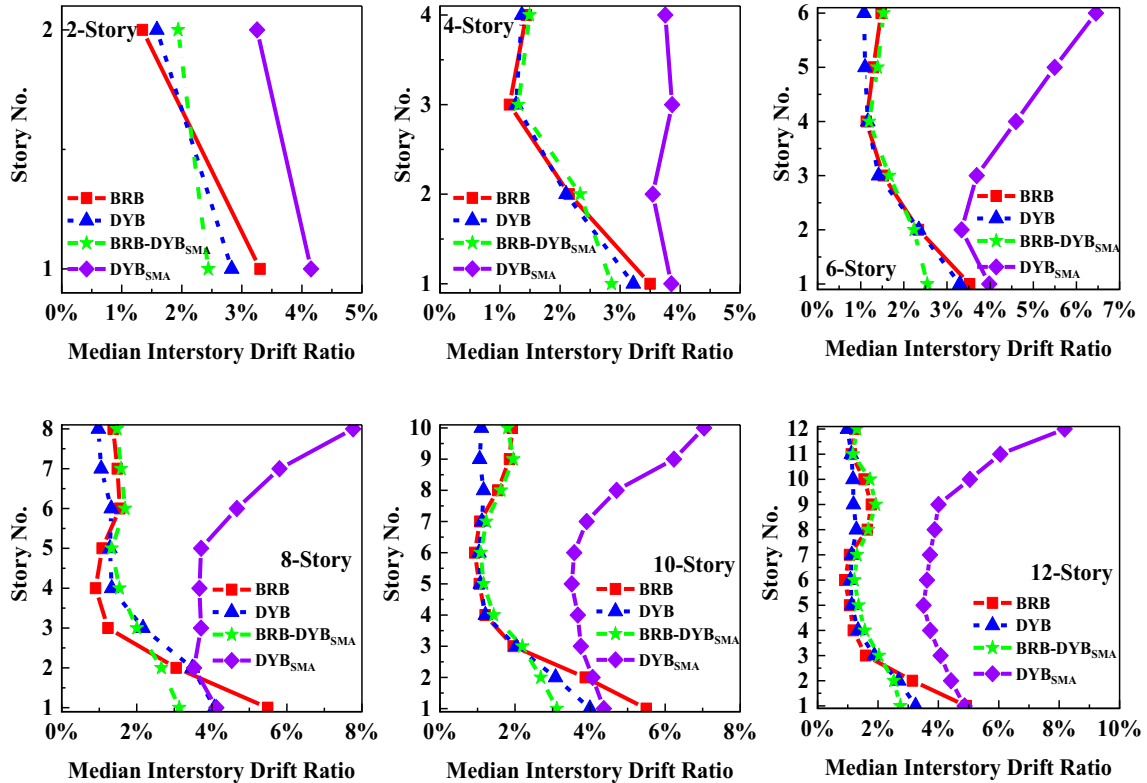

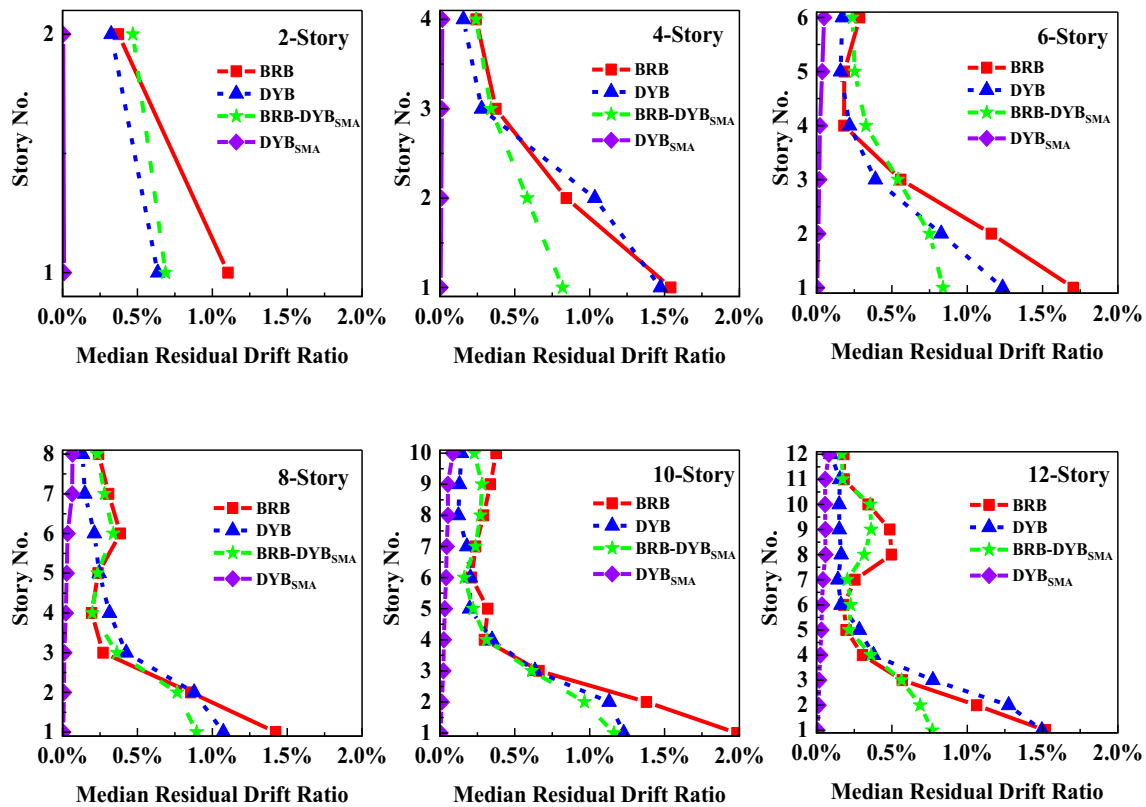**Fig. 13** IDR$_{Med}$ of BRBFs considering different lateral systems under MCE level

Fig. 14 RDR_{Med} of BRBFs considering different lateral systems under MCE level

BRB and DYB systems, respectively. In addition, the BRB-DYB_{SMA} can decrease the RDR_{Med} by 97.78% and 94.79% compared to BRB and DYB systems, respectively. Therefore, it can be observed that the BRB-DYB_{SMA} system can considerably reduce both demands and is recommended for MCE-level ground motions.

The results of analysis confirmed that the DYB_{SMA} system has the largest values of IDR_{Med} and the lowest values of RDR_{Med} compared to other lateral systems, which is the result of the self-centering ability of SMA materials. Since the all systems have been designed as retrofitting purpose and they are implemented on the BRBFs, they have same design target and the seismic behavior of the structure stems from its lateral force-resisting system. Although the DYB_{SMA} had the lowest permanent deformations, this system experienced the highest values of lateral deformations and do not have a good performance in this demand under DBE and MCE levels.

3.4 Drift concentration

In order to quantify the distribution of the IDR_{Med} and RDR_{Med} demands in floor levels of all BRBFs, the drift concentration factor (DCF) is defined assuming the following formula:

$$DCF = \frac{\delta_{\max,floor_i}}{\delta_{\max,roof}} \qquad (5)$$

where the $\delta_{\max,floor_i}$ and $\delta_{\max,\ roof}$ present the maximum interstory drift of the floor level and the maximum drift of roof, respectively. According to Eq. (3), DCF equal to 1.0 can imply an ideal distribution, which shows an ideal sway mechanism. In addition, DCF greater or lower than 1.0 illustrates the weak and strong story, respectively. Figures 15 and 16 present DCF distribution for all BRBFs assuming different lateral systems under DBE and MCE levels, respectively. In DBE and MCE levels, the DYB_{SMA} system had the DCF approximately equal to 1.0 in 2-story and 4-story BRBFs, while by increasing the number of floor levels (i.e., 6-story to 12-story BRBFs), the DCF increased in upper floors that show the weak story levels. Comparing other lateral systems, DYB system had better DCF values in upper floor levels, while on lower floors (i.e., first and second floors), the DCF in greater than 1.0.

In addition, the BRB and BRB-DYB_{SMA} systems had a similar trend of DCF distributed in floor levels, which means the small effects of DYB_{SMA}. It can be concluded that the
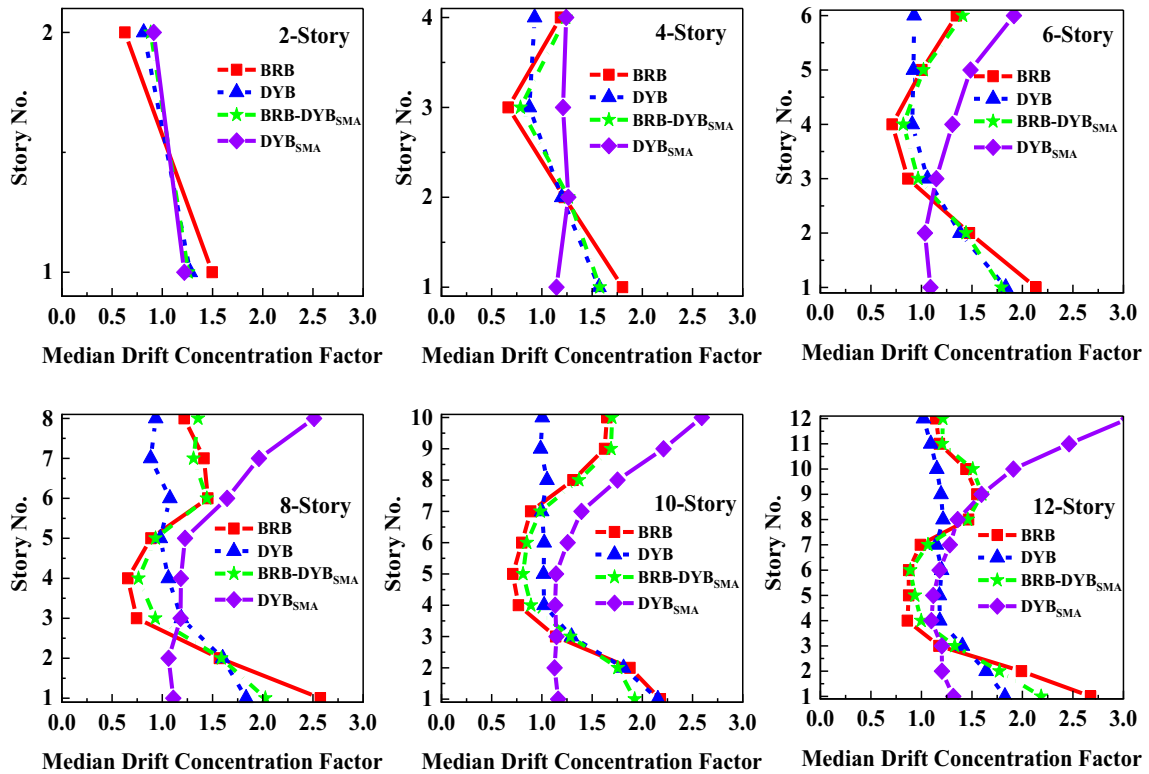
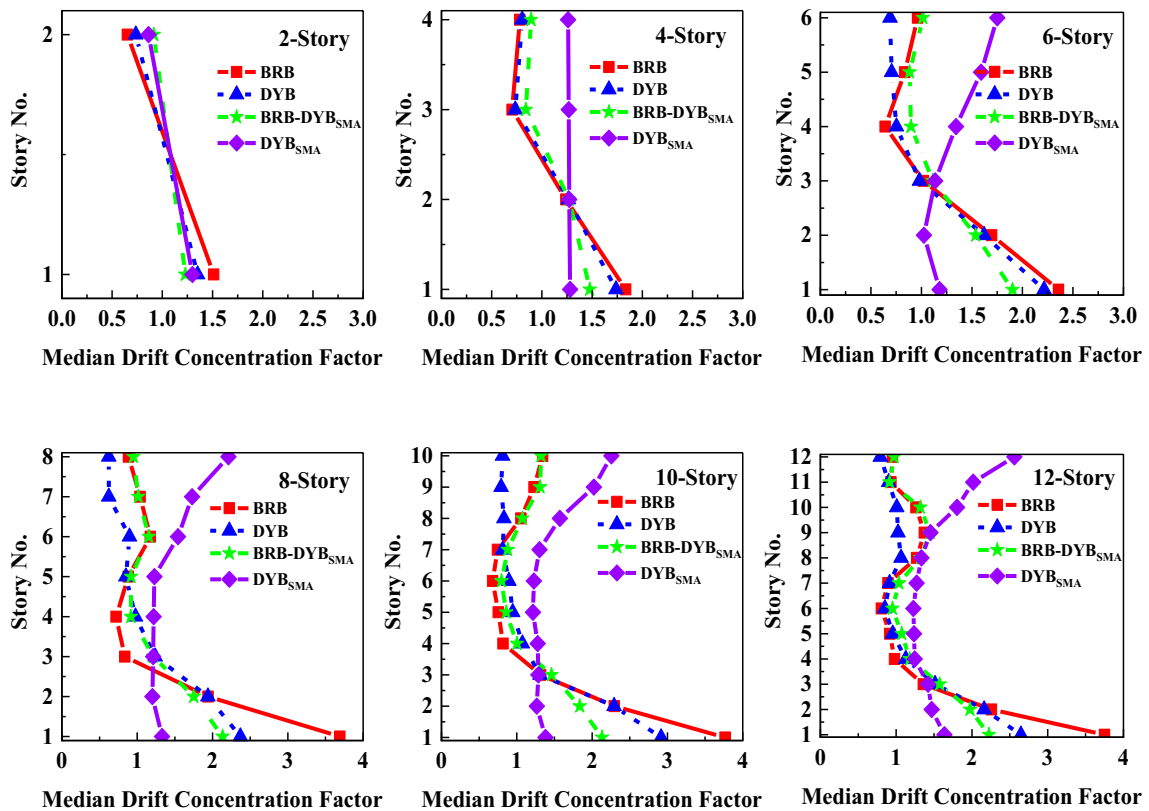**Fig. 15** IDR_{Med} of BRBFs considering different lateral systems under the DBE level

Fig. 16 RDR_{Med} of BRBFs considering different lateral systems under MCE level

proposed DYB system is suffer from a weak story in lower floor levels (i.e., first and second floors), while it shows a good performance with ideal DCF on upper floors.

3.5 IDA curves

To achieve the performance of assumed BRBFs, IDAs were performed considering the IDR as controlling demand. Although there are many scalar intensity measures for performing IDAs, some studies showed that the spectral acceleration at the fundamental period of structures (i.e., $S_a(T_1)$) has acceptable efficiency and sufficiency, and the results are reliable (see for instance [41, 42]). Figure 17 depicts the IDA curves of the 2-story BRBFs considering (a) BRB, (b) DYB,

(c) BRB-DYB$_{SMA}$, and (d) DYB$_{SMA}$, as lateral-resisting systems. It is noteworthy that the IDR of 10% was selected to have the collapse state of structures, in which, the BRBFs are losing their strength and there are structural damages that confirms the structure meet the condition of collapse state. Therefore, there is no need to monitor further engineering demands.

The Median of $Sa_{Collapse}(T_1)$ and the logarithmic standard deviation of the $Sa_{Collapse}(T_1)$ ($\sigma_{lnSaCol}$) for all BRBFs are presented in Table 4. The DYB system implemented in 2 to 12-story BRBFs increased the Median of $Sa_{Collapse}(T_1)$ values by 1.26, 1.07, 1.10, 1.31, 1.13, and 1.21 times, respectively, while implementing the BRB-DYB$_{SMA}$, the Median of $Sa_{Collapse}(T_1)$ values improved by 1.38, 1.55, 1.73, 2.02,
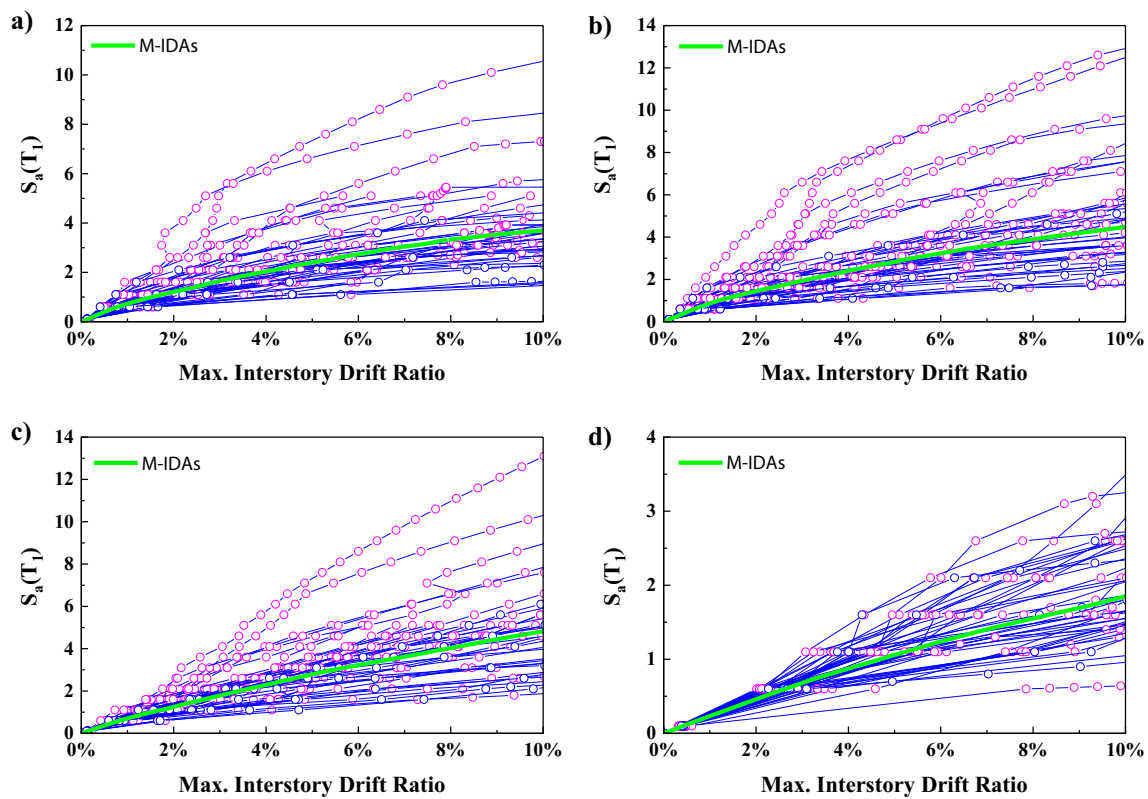

Fig. 17 IDA curves of the 2-story BRBFs considering, **a** BRB, **b** DYB, **c** BRB-DYB$_{SMA}$, and **d** DYB$_{SMA}$, as lateral systems

Table 4 Median of $Sa_{Collapse}(T_1)$ and the logarithmic standard deviation of the $Sa_{Collapse}(T_1)$ for all BRBFs

BRBFs	Median of $Sa_{Collapse}(T_1)$				$\sigma_{lnSaCol}$			
	BRB	DYB	BRB-DYB$_{SMA}$	DYB$_{SMA}$	BRB	DYB	BRB-DYB$_{SMA}$	DYB$_{SMA}$
2-Story	3.999	5.049	5.527	2.185	0.439	0.505	0.459	0.368
4-Story	2.11	2.259	3.278	1.594	0.405	0.43	0.381	0.409
6-Story	1.232	1.357	2.129	0.802	0.49	0.493	0.479	0.365
8-Story	0.661	0.863	1.335	0.594	0.446	0.424	0.517	0.439
10-Story	0.557	0.629	1.018	0.451	0.383	0.444	0.468	0.537
12-Story	0.46	0.555	0.801	0.375	0.405	0.433	0.456	0.501

1.83, and 1.74 times, respectively. Therefore, the DYB and BRB-DYB$_{SMA}$ systems have increased the Median of Sa$_{Collapse}$(T$_1$) by an average of 18% (from 7% to 31%) and 71% (from 38% to 102%), respectively.

Comparing the results of the Median of Sa$_{Collapse}$(T$_1$) show that the DYB$_{SMA}$ system achieved the lowest values compared to other systems, which means this system collapsed earlier than others. In addition, the DYB$_{SMA}$ system implemented in 2- to 12-story BRBFs decreased the Median of Sa$_{Collapse}$(T$_1$) values by 45.4%, 24.5%, 34.9%, 10.1%, 19.0%, and 18.5%, respectively, compared to BRB system. Moreover, the DYB$_{SMA}$ system, which was created using the SMA material, has a negative effect on the performance of BRBFs. It is observed that the DYB$_{SMA}$ system implemented in 2- to 12-story BRBFs decreased the Median of Sa$_{Collapse}$(T$_1$) values by 56.7%, 29.4%, 40.9%, 31.2%, 28.3%, and 32.4%, respectively, compared to DYB system.

3.6 Collapse margin ratio

Collapse margin ratio (CMR) can be assumed as a safety factor for the collapse of structures under the MCE level. To determine the CMR, the following formula can be used:

$$CMR = \frac{\text{Median}(Sa_{Collapse,i})}{Sa_{MCR}} \quad (6)$$

where the Median of Sa$_{Collapse}$(T$_1$) can be determined from Table 4, and Sa$_{MCR}$ can be achieved from the design spectrum under the MCE level corresponding to the fundamental period of BRBFs. Table 5 illustrates the CMR values of BRBFs under MCE-level ground motions. All determined values of CMR are upper than 1.0 which means there is a safety margin for all considered BRBFs under MCE-level ground motions. It can be seen that by increasing the elevation of BRBFs, the CMR values decreased, while different systems lead to different values of CMR. Comparing all the CMR values with the BRB system, the CMR values in the 2- to 12-story BRBFs with the DYB system increased by 1.22,

Table 5 The CMR values of BRBFs under MCE level ground motions

BRBFs	BRB	DYB	BRB-DYB$_{SMA}$	DYB$_{SMA}$
2-Story	2.31	2.81	3.5	2.21
4-Story	2.09	2.23	3.24	2.6
6-Story	1.74	1.94	3	1.93
8-Story	1.23	1.63	2.49	1.8
10-Story	1.26	1.44	2.31	1.66
12-Story	1.22	1.5	2.15	1.61

1.07, 1.11, 1.33, 1.14, and 1.23 times, respectively, while the BRB-DYB$_{SMA}$ system increased the CMR values 1.52, 1.55, 1.72, 2.02, 1.83, 1.76 times, respectively. In addition, using DYB$_{SMA}$ system can increase the CMR values of 2- to 12-story BRBFs by 0.96, 1.24, 1.11, 1.46, 1.32, and 1.32 times, respectively. It is confirmed that using SMA materials has a positive influence on the CMR values; hence, the kind of implementation of SMA materials is important for performance assessment.

3.7 Fragility curves

The fragility curve can be defined as the exceedance probability of an engineering demand (i.e., collapse state) as a function of intensity measure (i.e., Sa(T$_1$)). In this study, the collapse state of BRBFs was assumed as a demand parameter and the fragility curves were determined based on them. To better compare the fragility curves of BRBFs, the horizontal axes of the fragility curves were normalized to the Sa$_{MCR}$, which defines the design spectrum under the MCE level corresponding to the fundamental period of BRBFs. Figure 18 presents the normalized fragility curves of BRBFs considering four cases of lateral systems. Considering the probability of collapse equal to 50%, the BRB, DYB, BRB-DYB$_{SMA}$, and DYB$_{SMA}$ implemented in 2-story BRBF had the normalized Sa(T$_1$)/Sa$_{MCE}$(T$_1$) values of 2.32, 2.81, 3.50, and 2.96, respectively. In addition, the BRB, DYB, BRB-DYB$_{SMA}$, and DYB$_{SMA}$ implemented in 4-story BRBF had the normalized Sa(T$_1$)/Sa$_{MCE}$(T$_1$) values of 2.11, 2.24, 3.25, and 2.62, respectively. For 6-story BRBF, the BRB, DYB, BRB-DYB$_{SMA}$, and DYB$_{SMA}$ systems had the normalized Sa(T$_1$)/Sa$_{MCE}$(T$_1$) values of 1.76, 1.96, 3.03, and 2.14, respectively, and for 8-story BRBF, the normalized Sa(T$_1$)/Sa$_{MCE}$(T$_1$) values of 1.25, 1.64, 2.52, and 1.84, respectively, were determined. Similarly, the BRB, DYB, BRB-DYB$_{SMA}$, and DYB$_{SMA}$ implemented in 10-story BRBF had the normalized Sa(T$_1$)/Sa$_{MCE}$(T$_1$) values of 1.26, 1.44, 2.33, and 1.72, respectively, while the normalized Sa(T$_1$)/Sa$_{MCE}$(T$_1$) values for 12-story BRBF were equal to 1.25, 1.54, 2.17, and 1.59, respectively.

It can be seen that in all BRBFs, the BRB system had the lowest values of the normalized Sa(T$_1$)/Sa$_{MCE}$(T$_1$) which shows the highest probability of collapse occurrence. While the BRB-DYB$_{SMA}$ had the highest values of the normalized Sa(T$_1$)/Sa$_{MCE}$(T$_1$) that confirms the lowest probability of collapse occurrence. It can be seen that the DYB and DYB$_{SMA}$ have a good performance in the BRBFs and these two systems can be employed to reduce the probability of collapse occurrence.

The results showed that the SMA materials used in DYB brace (i.e., DYB$_{SMA}$) can highly influence the probability of collapse occurrence; hence, using the mixed braces (i.e., BRB-DYB$_{SMA}$) have better results than employing the same
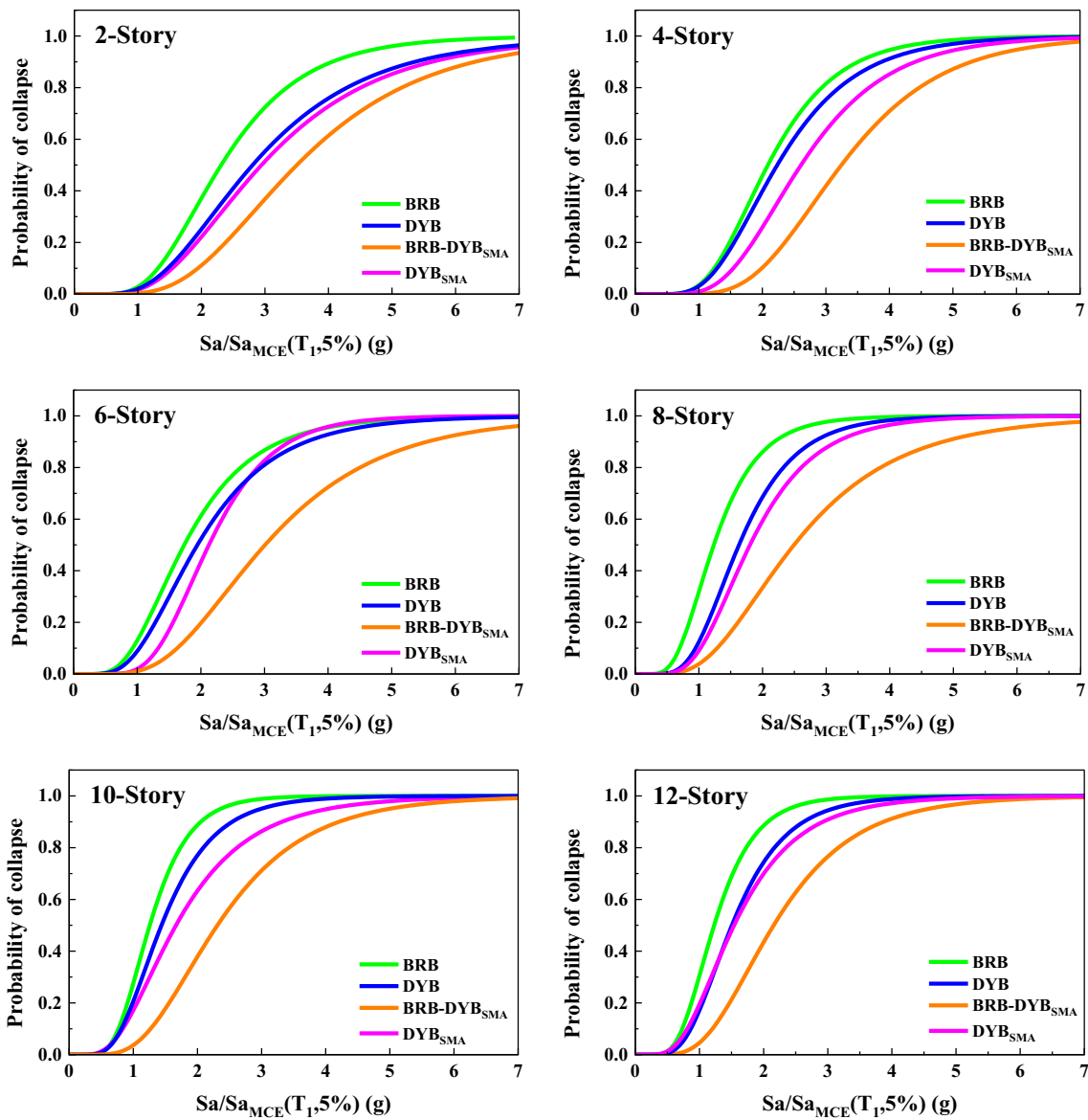
Fig. 18 Normalized fragility curves of BRBFs considering four cases of lateral systems

brace systems. For example, although the DYB_{SMA} system improved the probability of collapse occurrence in the 8-story BRBF by 47.2%, using the BRB-DYB_{SMA} system have better improvement by 101.6% compared to the BRB system.

3.8 Annual frequency of exceedance

The mean annual frequency of collapse level, λ_{Col}, can be determined based on the seismic hazard curves of the located site of BRBFs and the fundamental period of structures. Figure 19 presents the seismic hazard curves of the construction site assumed for BRBFs. These curves were used for the interpolation of hazard curves for the fundamental period
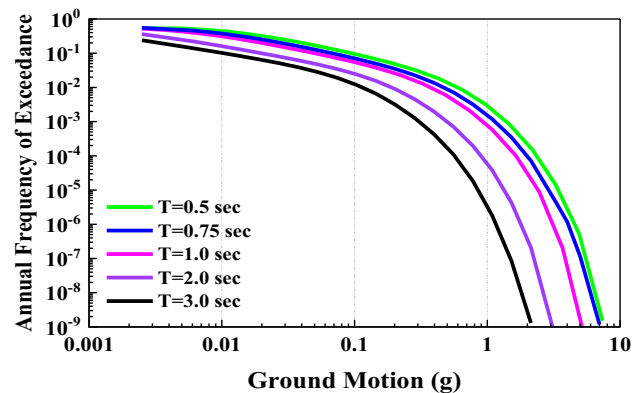
Fig. 19 Seismic hazard curves of the construction site assumed for BRBFs

of BRBFs. Then, using these curves and fragility curves, it is possible to calculate the λ_{Col}. To determine the λ_{Col}, the following formula can be used [35]:

$$\lambda_{Col} = \sum_{i=1}^{n} P(Collapse|Sa_i) \times \left| \frac{d\lambda_{Sa}(Sa_i)}{d(Sa)} \right| \times \Delta(Sa) \qquad (7)$$

where the $P(Collapse|Sa_i)$ defines the fragility curve based on the collapse state and the $\left| \frac{d\lambda_{Sa}(Sa_i)}{d(Sa)} \right|$ presents the slope of hazard curves presented in Fig. 19.

The λ_{Col} expresses the mean yearly rate of collapse of the building and is equal to the area of the deaggregation curves, which are presented in Fig. 20. As can be observed from Fig. 20, the area of the curves presented for the BRB-DYB_{SMA} system for all BRBFs is much lower than the other systems. While the DYB_{SMA} has the highest area for 2-story BRBF, the BRB system has the highest area for other BRBFs. It can be seen that innovative systems can decrease the λ_{Col} to reduce the rate of collapse per year.

Table 6 illustrates the λ_{Col} values determined from the deaggregation curves of BRBFs in Fig. 20 considering four lateral systems. Since the λ_{Col} defines the collapse rate per year, as low as possible values can guarantee the building against external excitations against collapse occurrence. Therefore, the BRB-DYB_{SMA} that has the lowest values of

Table 6 λ_{Col} values determined from deaggregation curves of BRBFs considering four lateral systems

BRBFs	BRB ($\times 10^{-5}$)	DYB ($\times 10^{-5}$)	BRB-DYB-$_{SMA}$ ($\times 10^{-5}$)	DYB_{SMA} ($\times 10^{-5}$)
2-Story	5.28	3.51	1.11	12.4
4-Story	18.73	16.5	2.08	13.1
6-Story	77.36	55.53	10.68	33
8-Story	178.16	77.3	28.81	45.1
10-Story	140.53	110.95	28.4	66.25
12-Story	137.7	83.54	30.1	62.8

λ_{Col} can be considered the best lateral-resisting system in all BRBFs. Although the DYB system can highly decrease the amount of λ_{Col} compared to the BRB system, adding SMA materials can improve the performance of DYB more effectively. For instance, the DYB_{SMA} system can decrease the λ_{Col} values of 4-, 6-, 8-, 10- and 12-story BRBF having BRB system by 30.05%, 57.34%, 74.68%, 52.85%, and 54.39% respectively. It can be seen that by increasing the number of stories, the effectiveness of the proposed systems is more evident.
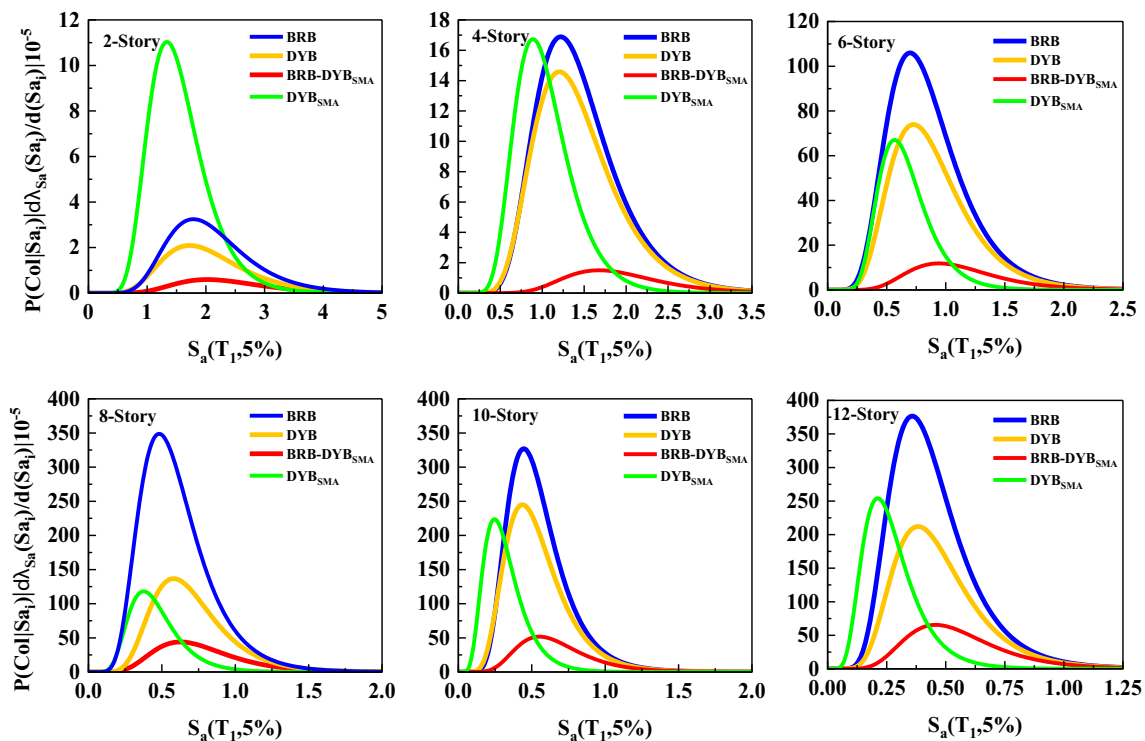
Fig. 20 Deaggregation curves of BRBFs considering four lateral systems

Table 7 Collapse probability occurrence over 1 and 50 years for all BRBFs

BRBFs	P_C (per year) %				P_C (per 50 years) %			
	BRB	DYB	BRB-DYB$_{SMA}$	DYB$_{SMA}$	BRB	DYB	BRB-DYB$_{SMA}$	DYB$_{SMA}$
2-Story	0.005	0.003	0.001	0.012	0.264	0.175	0.055	0.616
4-Story	0.019	0.016	0.002	0.013	0.932	0.821	0.104	0.653
6-Story	0.077	0.055	0.01	0.033	3.794	2.738	0.532	1.637
8-Story	0.178	0.077	0.029	0.045	8.523	3.791	1.43	2.227
10-Story	0.14	0.111	0.028	0.066	6.785	5.396	1.41	3.258
12-Story	0.138	0.083	0.03	0.062	6.653	4.091	1.493	3.093

The values of λ_{Col} can be used for calculating the collapse probability occurrence over 1 and 50 years. Table 7 illustrates the collapse probability occurrence over 1 and 50 years for all BRBFs calculated by λ_{Col} values presented in Table 6. Similarly, the proposed systems have lower collapse probability occurrence over 1 and 50 years compared to the BRB system. In addition, the lowest values of collapse probability occurrence over 1 and 50 years belong to the BRB-DYB$_{SMA}$. Moreover, the DYB and DYB$_{SMA}$ can be used for improving the BRB system as they have better results.

4 Conclusion

This study investigates three proposed innovative lateral-resisting systems that can be replaced for the BRB system. The proposed systems have been verified and implemented in 2- to 12-story elevation BRBFs to evaluate their effects on the structures. To better present the efficiency of proposed lateral-resisting systems, two types of analysis including NDAs and IDAs were performed considering DBE and MCE levels for far-field ground motions. The points of analysis results are presented in the following sentences:

- Increasing the gap distance in numerical models can considerably increase the RDR$_{Med}$, which shows the significant influence of the small part of DYB. Therefore, the appropriate values of gap distance for controlling the IDR$_{Med}$ and RDR$_{Med}$ demands are proposed.
- Under the MCE level, the results show that the BRB-DYB$_{SMA}$ structures had lower values of the IDR$_{Med}$ and RDR$_{Med}$ demands. For instance, the BRB-DYB$_{SMA}$ in a 12-story structure can reduce the IDR$_{Med}$ by 79.67% and 18.5% compared to BRB and DYB systems, respectively. Moreover, the BRB-DYB$_{SMA}$ can decrease the RDR$_{Med}$ by 97.78% and 94.79% compared to BRB and DYB systems, respectively.
- In DBE and MCE levels, the DYB$_{SMA}$ system had the DCF approximately equal to 1.0 in 2-story and 4-story BRBFs, and by increasing floor levels (i.e., 6-story to 12-story BRBFs), BRBFs suffer from weak story levels

and have higher values of DCF. On the other hand, the DYB system had better DCF values on upper floor levels. Due to the small effects of DYB$_{SMA}$, the BRB and BRB-DYB$_{SMA}$ systems had a similar trend of DCF distributed in floor levels.

- The DYB and BRB-DYB$_{SMA}$ systems have increased the Median of Sa$_{Collapse}$(T$_1$) by an average of 18% (from 7 to 31%) and 71% (from 38 to 102%), respectively. The results showed that using SMA material has a negative effect on the performance of BRBFs. For instance, in the Median of Sa$_{Collapse}$(T$_1$) values for 2- to 12-story BRBFs decreased by 56.7%, 29.4%, 40.9%, 31.2%, 28.3%, and 32.4%, respectively, for using the DYB$_{SMA}$ system instead of the DYB system.
- It is confirmed that using SMA materials has a positive influence on the CMR values; hence, using the DYB$_{SMA}$ alone has lower effects than using it by the BRB system (i.e., BRB-DYB$_{SMA}$).
- The results showed that the SMA materials used in DYB brace (i.e., DYB$_{SMA}$) can highly influence the probability of collapse occurrence; hence, using the mixed braces (i.e., BRB-DYB$_{SMA}$) have better results than employing the same brace systems.
- The results of the λ_{Col}, which defines the collapse rate per year, showed that the BRB-DYB$_{SMA}$ system for all BRBFs has lower values than the other systems, which can be considered as the best proposed lateral-resisting system. In addition, it can be seen that innovative systems can decrease the λ_{Col} to reduce the rate of collapse per year.

Declarations

References

1. Tabatabaei SA, Mirghaderi SR, Hosseini A. Experimental and numerical developing of reduced length buckling-restrained braces. Eng Struct. 2014;15(77):143–60.
2. Mortezagholi MH, Zahrai SM. Analytical and numerical studies on reducing lateral restraints in conventional & all steel buckling restrained braces. J Build Eng. 2020;1(32): 101513.
3. Pandikkadavath MS, Sahoo DR. Cyclic testing of short-length buckling-restrained braces with detachable casings. Earthq Struct. 2016;10(3):699–716.
4. Hosseinzadeh S, Mohebi B. Seismic evaluation of all-steel buckling restrained braces using finite element analysis. J Constr Steel Res. 2016;1(119):76–84.
5. Judd JP, Marinovic I, Eatherton MR, Hyder C, Phillips AR, Tola AT, Charney FA. Cyclic tests of all-steel web-restrained buckling-restrained brace subassemblages. J Constr Steel Res. 2016;1(125):164–72.
6. Tong JZ, Guo YL. Numerical investigations on elastic buckling and hysteretic behavior of steel angles assembled buckling-restrained braces. J Constr Steel Res. 2018;1(144):21–39.
7. Jia LJ, Ge H, Maruyama R, Shinohara K. Development of a novel high-performance all-steel fish-bone shaped buckling-restrained brace. Eng Struct. 2017;1(138):105–19.
8. Yakhchalian M, Yakhchalian M, Asgarkhani N. An advanced intensity measure for residual drift assessment of steel BRB frames. Bull Earthq Eng. 2021;19:1931–55.
9. Asgarkhani N, Yakhchalian M, Mohebi B. Evaluation of approximate methods for estimating residual drift demands in BRBFs. Eng Struct. 2020;1(224): 110849.
10. Kazemi F, Jankowski R. Seismic performance evaluation of steel buckling-restrained braced frames including SMA materials. J Constr Steel Res. 2023;1(201): 107750.
11. Zhang S, Tagawa H, Chen X. Study on buckling-restrained braces using multiple round steel core bars. J Constr Steel Res. 2022;1(199): 107573.
12. Mateus JA, Tagawa H, Chen X. Buckling-restrained brace using round steel bar cores restrained by inner round steel tubes and outer square steel tube. Eng Struct. 2019;15(197): 109379.
13. Bai J, Chen H, Jin S, You T. Development of dual-parameter loading protocols for buckling-restrained braced RC frames considering variable axial loads. Eng Struct. 2022;1(262): 114388.
14. Zhang Y, Ren X, Zhang XY, Huang TT, Sun L, Xie YM. A novel buckling-restrained brace with auxetic perforated core: Experimental and numerical studies. Eng Struct. 2021;15(249): 113223.
15. Sun J, Pan P, Wang H. Development and experimental validation of an assembled steel double-stage yield buckling restrained brace. J Constr Steel Res. 2018;1(145):330–40.
16. Hu B, Min Y, Wang C, Xu Q, Keleta Y. Design, analysis and application of the double-stage yield buckling restrained brace. J Build Eng. 2022;1(48): 103980.
17. Miller DJ, Fahnestock LA, Eatherton MR. Development and experimental validation of a nickel–titanium shape memory alloy self-centering buckling-restrained brace. Eng Struct. 2012;1(40):288–98.
18. Ghowsi AF, Sahoo DR. Near-field earthquake performance of SC-BRBs with optimal design parameters of SMA. J Constr Steel Res. 2020;1(175): 106321.
19. Shi F, Saygili G, Ozbulut OE. Probabilistic seismic performance evaluation of SMA-braced steel frames considering SMA brace failure. Bull Earthq Eng. 2018;16:5937–62.
20. Shi F, Saygili G, Ozbulut OE, Zhou Y. Risk-based mainshock-aftershock performance assessment of SMA braced steel frames. Eng Struct. 2020;212: 110506.
21. Shi F, Zhou Y, Ozbulut OE, Ren F. Hysteretic response and failure behavior of an SMA cable-based self-centering brace. Struct Control Health Monit. 2022;29(1): e2847.
22. Kong S, Shi F, Zhou Y, Ma Y, Xie L. Influence of BRBs deformation capacity on the seismic performance of RC building frames. Soil Dyn Earthq Eng. 2022;161: 107442.
23. Shi F, Lin Z, Li Q, Ozbulut OE, He Z, Zhou Y. Design, manufacturing, and testing of a hybrid self-centering brace for seismic resilience of buildings. Earthq Eng Struct Dynam. 2023;52(5):1381–402.
24. Barbagallo F, Bosco M, Marino EM, Rossi PP. Achieving a more effective concentric braced frame by the double-stage yield BRB. Eng Struct. 2019;186:484–97.
25. Kiggins S, Uang CM. Reducing residual drift of buckling-restrained braced frames as a dual system. Eng Struct. 2006;28(11):1525–32.
26. Marshall JD, Charney FA. Seismic response of steel frame structures with hybrid passive control systems. Earthq Eng Struct Dynam. 2012;41(4):715–33.
27. Qiu C, Du X. Seismic performance of multistory CBFs with novel recentering energy dissipative braces. J Constr Steel Res. 2020;1(168): 105864.
28. Zhu R, Guo T, Tesfamariam S. Residual displacement demand for non-degrading bilinear SDOF oscillators with self-centering viscous-hysteretic devices. Soil Dyn Earthq Eng. 2022;1(155): 107189.
29. McKenna F, Fenves GL, Filippou FC, Scott MH. Open system for earthquake engineering simulation (OpenSees). Berkeley: Pacific

Earthquake Engineering Research Center, University of California; 2005.

30. Qiu CX, Zhu S. Performance-based seismic design of self-centering steel frames with SMA-based braces. Eng Struct. 2017;1(130):67–82.

31. Kazemi F, Jankowski R. Enhancing seismic performance of rigid and semi-rigid connections equipped with SMA bolts incorporating nonlinear soil-structure interaction. Eng Struct. 2023;1(274): 114896.

32. ASCE 7-10. Minimum design loads and associated criteria for buildings and other structures. Reston: American Society of Civil Engineers; 2010.

33. AISC Committee. Specification for structural steel buildings (ANSI/AISC 360-10). Chicago-Illinois: American Institute of Steel Construction; 2010.

34. AISC, A. AISC 341-10, seismic provisions for structural steel buildings. Chicago, IL: American Institute of Steel Construction; 2010.

35. Kazemi F, Asgarkhani N, Jankowski R. Machine learning-based seismic response and performance assessment of reinforced concrete buildings. Arch Civil Mech Eng. 2023;23(2):94.

36. Asgarkhani N, Kazemi F, Jankowski R. Optimal retrofit strategy using viscous dampers between adjacent RC and SMRFs prone to earthquake-induced pounding. Arch Civil Mech Eng. 2022;23(1):7.

37. Kazemi F, Jankowski R. Machine learning-based prediction of seismic limit-state capacity of steel moment-resisting frames considering soil-structure interaction. Comput Struct. 2023;1(274): 106886.

38. Kazemi F., Asgarkhani N, Jankowski R. Predicting seismic response of SMRFs founded on different soil types using machine learning techniques. Eng Struct. 2023;1(274): 114953.

39. Kazemi F, Asgarkhani N, Jankowski R. Probabilistic assessment of SMRFs with infill masonry walls incorporating nonlinear soil-structure interaction. Bull Earthq Eng. 2023;21(1):503–34.

40. Kazemi F, Asgarkhani N, Jankowski R. Machine learning-based seismic fragility and seismic vulnerability assessment of reinforced concrete structures. Soil Dyn Earthq Eng. 2023;1(166): 107761.

41. Kazemi F., Asgarkhani N, Manguri A, Lasowicz N, Jankowski R. Introducing a Computational Method to Retrofit Damaged Buildings under Seismic Mainshock-Aftershock Sequence. In: International Conference on Computational Science; 2023 Jun 26. pp. 180–187.

42. Applied Technology Council (FEMA P695). Quantification of building seismic performance factors. US Department of Homeland Security, FEMA; 2009.